Received: 23 May 2023 | Revised: 10 January 2024 | Accepted: 11 January 2024

DOI: 10.1002/pol.20230332

RESEARCH ARTICLE

JOURNAL OF POLYMER SCIENCE WILEY

Kinetics of nanoconfined benzyl methacrylate radical polymerization

Chunhao Zhai[1] | **Yung P. Koh**[2] | **Bryan D. Vogt**[3] | **Sindee L. Simon**[2]

[1]Department of Chemical Engineering, Texas Tech University, Lubbock, Texas, USA

[2]Department of Chemical and Biomolecular Engineering, North Carolina State University, Raleigh, North Carolina, USA

[3]Department of Chemical Engineering, The Pennsylvania State University, University Park, Pennsylvania, USA

Correspondence
Sindee L. Simon, Department of Chemical and Biomolecular Engineering, North Carolina State University, Raleigh, NC 27695, USA.
Email: slsimon@ncsu.edu

Funding information
National Science Foundation, Grant/Award Numbers: DMR-2141221, DMR-2004960, DMR-1610614; Division of Chemical, Bioengineering, Environmental, and Transport Systems, Grant/Award Numbers: 1510612, 1336057; The Horn Professorship of Texas Tech University

Abstract

The effect of nanoconfinement on the kinetics of benzyl methacrylate radical polymerization is investigated using differential scanning calorimetry. Controlled pore glass (CPG), ordered mesoporous carbons, and mesoporous silica are used as confinement media with pore sizes from 2 to 8 nm. The initial polymerization rate in CPG and mesoporous silica increases relative to the bulk and increases linearly with reciprocal pore size; whereas, the rate in the carbon mesopores decreases linearly with reciprocal pore size; the changes are consistent with the rate being related to the ratio of the pore surface area to pore volume. Induction times are longer for nanoconfined polymerizations, and in the case of CPG and carbon mesopores, autoacceleration occurs earlier, presumably due to the limited diffusivity and lower termination rates for the confined polymer chains. The molecular weight of the polymer synthesized in the nanopores is generally higher than that obtained in the bulk except at the lowest temperatures investigated. The equilibrium conversion under nanoconfinement decreases with decreasing temperature and with confinement size, exhibiting what appears to be a floor temperature at low temperatures.

KEYWORDS

nanoconfinement, poly(benzyl methacrylate), polymerization, reaction kinetics

1 | INTRODUCTION

Nanoconfinement is well known to affect the properties of materials, including the melting temperature[1–3] and the glass transition temperature (T_g),[4–8] as well as drastically changing the kinetics of radical polymerization in heterogeneous emulsion and miniemulsion polymerizations.[9–11] In the last two decades, the effect of nanoconfinement on the kinetics of homogeneous polymerizations have been investigated,[5,7,12–19] and they are quite different from those in dispersed phase polymerizations. For example, termination in nanoconfined homogenous radical polymerization is dominated by the bimolecular chain termination mechanism and is impacted by changes in diffusion under nanoconfinement, whereas termination in emulsion polymerization is generally controlled by the rate at which initiator radicals from the continuous phase enter the dispersed monomeric phase. In addition, the large surface area of nanopores may also impact the rate of reaction in nanopore-confined polymerizations. Zhao and Simon[12] recently reviewed the influence of hard nanoconfinement on different types of homogeneous polymerizations, as

well as on the properties of polymers synthesized in nanoreactors. For step-growth polymerizations of phenolic resin,[13] isocyanate,[14] cyanate ester,[5,7,15–17] and epoxy,[18] the reaction rate is generally accelerated under nanoconfinement. The increase in reactivity can be attributed to catalysis by functional groups on the pore surface and/or to layering of monomer at the pore walls resulting in a higher local concentration of functional groups.[19] On the other hand, for nanoconfined radical polymerizations, prior investigations have focused on vinyl monomers.[20–26] In our laboratory,[20–22] polymerization of methyl methacrylate (MMA), ethyl methacrylate (EMA), butyl methacrylate (BMA), and dodecyl methacrylate (DMA) have been studied in controlled pore glass (CPG) with diameters from 4 to 111 nm using differential scanning calorimetry (DSC). The rate of polymerization is higher in native CPG relative to bulk and inversely proportional to the pore size; this enhanced reaction rate under nanoconfinement is largest for MMA and weakest for DMA and appears to change linearly with decreasing length of the alkyl group and increasing monomer hydrophobicity.[23] In contrast to our work in CPG, several groups have also performed nanoconfined radical polymerizations in the pores of anodic aluminum oxide membranes (AAO),[24–26] and although a higher reaction rate was observed for styrene in AAO,[24] both vinyl pyrrolidone and a fluorinated acrylic showed reduced rates of polymerization.[25,26] On the other hand, studies on nanoconfined reversible deactivation radical[27] and ring-opening[28,29] polymerizations also report increases in the rate of polymerization. In terms of properties, nanoconfinement often increases molecular weight and tacticity, while decreasing molar mass dispersity (Đ) in metal-organics frameworks (MOF) and CPG confinement,[27,30–35] although in AAO,[24–26] molecular weight and PDI have been found to be both lower than in the bulk.

In this study, the kinetics of homogeneous radical polymerization of benzyl methacrylate (BzMA) in bulk and under nanoconfinement is investigated. We choose to study BzMA because of its higher boiling point and lower volatility compared to the n-alkyl methacrylates[20,22,23] used in our previous work. Three different nanoconfinement media are examined, CPG, mesoporous silica, and ordered mesoporous carbon, the latter of which is made by templated synthesis of mesoporous materials resulting in narrow pore size distribution and relatively high specific pore volumes.[36–42] To the best of our knowledge, this is the first report to use mesoporous silica and mesoporous carbon as a confinement media for nanoconfined polymerization, and this is of interest in order to determine, as previously stated, the influence of confinement size versus other effects, such as those attributed to surface or surface functionality.

2 | EXPERIMENTAL METHOD

2.1 | Materials

BzMA monomer (96%, containing 50 ppm monomethyl ether hydroquinone as inhibitor) was purchased from Sigma Aldrich. The monomer was purified using a prepacked column (Sigma Aldrich 306,312) to remove the inhibitor. Polymerization was initiated with either 2,2′-azobisisobutyronitrile (AIBN) (Sigma Aldrich, 98%) at concentrations of 1.5 or 2.5 wt % or for higher temperature polymerizations with 0.5 wt % di-tert-butyl peroxide (DTBP) (Sigma Aldrich, 98%). Initiator was mixed with monomer to form a homogenous solution at room temperature, and then the solutions were stored in a container with desiccant at −20 °C prior to use. No significant conversion (<2%) occurred during storage.

The confinement media used included controlled pore glass (CPG) (Millipore) with nominal pore diameters of 4 and 8 nm and mesoporous silica (Sigma Aldrich) with pore diameters of 2, 4, and 8 nm. Prior to use, these materials were immersed in nitric acid (Mallinckrodt Chemicals, 68%–70%) at 110 °C for 10 h, then rinsed with water until neutral and dried under vacuum at 285 °C for 24 h. In addition, we used ordered mesoporous carbon[41] synthesized by cooperative assembly of phenolic resin and an amphiphilic triblock copolymer following prior reports[41–43] with details in the Data S1. Pore size, pore volume, and surface area for all four confinement matrices is summarized in Table 1. The large increase in the surface area for the 8 nm carbon material is primarily due to the presence of small micropores (<2 nm) that result from the removal of the silica.[43] From N_2 adsorption isotherms (shown in the Data S1), the volume of these small micropores is estimated to be 64% of the total

TABLE 1 Characteristics of confinement matrices.

Confinement matrix	Diameter (nm)	Specific pore volume (cm^3/g)	Surface area (m^2/g)[a]
CPG	4.0 ± 0.5	0.13	144
CPG	8.1 ± 0.7	0.49	197
Mesoporous silica	2.1 ± 0.2	0.1–0.4	900–1100
Mesoporous silica	4.0 ± 0.5	0.2–0.4	300–400
Mesoporous silica	8.0 ± 1.0	0.8–1.0	450–550
Mesoporous carbon	3.2 ± 0.5	0.26	395
Mesoporous carbon	8.3 ± 0.6	1.40	1505

[a]Surface area for ordered mesoporous carbons is from N_2 adsorption–desorption isotherms using a micromeritics tristar with pore volumes determined by the BJH method; for CPG and mesoporous silica, data is from the manufacturer.

porosity based on the volume of N_2 adsorbed prior to the hysteresis loop compared to the maximum N_2 adsorbed.

2.2 | DSC measurements

A Mettler–Toledo differential scanning calorimetry DSC 1 with an ethylene glycol cooling system and nitrogen purge is used to study the polymerization kinetics of the BzMA. 20 μL hermetic pans (Perkin Elmer) are used to minimize potential leakage during the reaction. All DSC samples are sealed under a nitrogen blanket to minimize adventitious moisture. For bulk samples, 3 to 7 mg of the monomer/initiator solution was put directly in the pan, whereas for nanoconfined samples, ~5–10 mg of matrix was placed on the bottom of the pan and then 1–3 mg of the monomer solution was placed on top using a syringe to deliver an amount such that the pore fullness ranged from 70% to 95%. This degree of pore fullness is not anticipated to influence the results because the monomer/initiator solution is anticipated to fill the CPG pores as a plug, as discussed by Jackson and McKenna,[44] and hence, there should be no influence on pore fullness on the measurements; for example, in prior work for the CPG-nanoconfined polymerization of cyanate ester, pore fullness was found to not influence either T_g values or trimerization reaction kinetics.[15,16] After the DSC runs, DSC pans for nanoconfined samples were opened and examined with no evidence of polymerization external to the confinement media, indicating full imbibement of the monomer in the porous media. Furthermore, we note that the porosity of the nanoconfinement matrix was unaffected by polymerization in the pores as there was no difference in the melting point depression of benzene in pores prior to polymerization and in pores in which the polymer has been extracted.[23]

The polymerizations of BzMA in bulk and under nanoconfinement were carried out isothermally at temperatures ranging from 50 °C to 120 °C and 100 °C to 190 °C for AIBN-initiated and DTBP-initiated samples, respectively. After polymerization in the DSC, <2% weight loss was observed for 95% of samples. Samples with >2% weight loss were excluded from further analysis and that data are not reported. The low volatility of the monomer, coupled with use of a limited temperature range, which reduces the risk of pan leakage, resulted in minimal monomer loss, which otherwise can be an important issue when dealing with higher volatility monomers.

The conversion of the monomer during isothermal polymerization (x) is calculated from the DSC heat flow ($\dot{Q}$):

$$x = \frac{1}{\Delta H_T}\int_{t_0}^{t} \dot{Q}dt \quad (1)$$

where the total heat of polymerization for 100% conversion, ΔH_T is taken to be 334 ± 6 J/g, based on bulk reactions at 60 °C to 100 °C, which is consistent with the literature value of 325 ± 5 J/g.[45] The heat of polymerization is theoretically a function of temperature as the heat capacities of both monomer and polymer change with temperature, but for BzMA polymerization, ΔH_T decreases by 1% over the temperature range of 373 to 463 K based on estimation of the heat capacities using the group contribution method[46]; for this reason, ΔH_T was considered constant.

The DSC temperature was calibrated with indium and (+)-4-*n*-hexylophenyl-40-(20-methylbutyl)-biphenyl-4-carboxylate (CE-3) at 10 K/min, and the enthalpy was calibrated with indium. An indium check run was performed daily to minimize instrumental error.

2.3 | GPC measurements

The molecular weight of the poly(benzyl methacrylate) (PBzMA) synthesized in bulk and in CPG and ordered mesoporous carbon was characterized using Tosoh HLC-8320GPC with TSKgel SuperH-H and two TSKgel SuperHM-H columns in series. Before the GPC measurements, the nanoconfined polymer was extracted from the confinement matrix using tetrahydrofuran (Sigma Aldrich, HPLC grade) for at least 48 h. The nanoconfinement matrix was removed using a Nylon Millex syringe filter (0.20 μm pore size, 13 mm diameter, Millex-GN Nylon membrane, hydrophilic). A refraction index (RI) detector was used to monitor the effluent stream and the molecular weight was calculated assuming a linear relationship between sample mass concentration and the RI response time. The GPC calibration curve was obtained from PMMA standards (Agilent Technologies) with molecular weights ranging from 2.71 to 1677 kg/mol; hence, the values are not absolute molecular weights but apparent values, relative to the PMMA standard. The calibration results were also checked using a PMMA standard before collecting data on the PBzMA samples, and the difference between the reported M_n of the standard and the measured M_n was <4%.

3 | RESULTS

Heat flow curves as a function of polymerization time at 90 °C for four representative samples containing 1.5 wt % AIBN initiator in bulk and in 3 or 4 nm-diameter nanopores are shown in Figure 1. In 4 nm CPG and 4 nm mesoporous silica, the initial heat flow is observed to be higher than in the bulk, indicating a higher reaction rate, consistent with our previous findings for *n*-alkyl polymerizations in hydrophilic native CPG nanopores.[20,22,23]

However, the polymerization in 3 nm mesoporous carbon shows a much lower exothermic peak, indicating a lower rate of polymerization than in the bulk. As indicated in Figure 1, we report the heat flow as a function of the reaction time after the induction time, t_{ind}, which is the time at which the exothermic reaction begins to occur; the induction time is easily determined from the raw heat flow data, as shown in the inset of Figure 1.

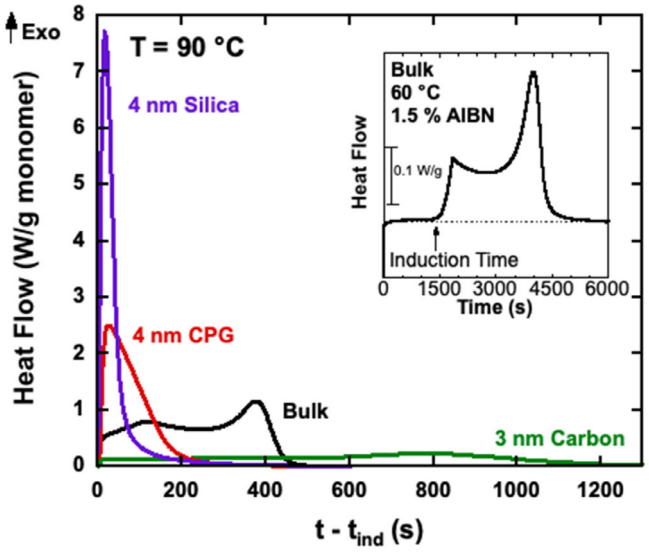

FIGURE 1 Representative heat flow as a function of isothermal reaction time (minus the induction time) at 90 °C for bulk and in 4 nm controlled pore glass, 4 nm mesoporous silica, and 3 nm ordered mesoporous carbon nanopores, all initiated by 1.5 wt % 2,2′-azobisisobutyronitrile. The inset shows a representative scan for bulk polymerization at 60 °C and how the induction time is determined.

The induction time is found to increase as reaction temperature decreases, as shown in Figure 2A, where the natural logarithm of the induction time is plotted versus the reciprocal temperature for AIBN-initiated samples, and in the inset for DTBP-initiated samples. At high temperatures, induction becomes too short to be observable, whereas at low temperatures, it can be as long as 10 h, for example, in 8 nm CPG at 50 °C. In general, the nanoconfined samples display longer induction times than the bulk samples, and this observation is consistent with our previous data for nanoconfined AIBN-initiated MMA polymerization,[20] as well as for DTBP-initiatied EMA and BMA polymerizations in native CPG,[22] although DTBP-initiatied DMA did not show significant differences from the bulk.[23]

The induction time for radical polymerization is suggested to be due to an inhibition reaction between a species A, such as oxygen, that quenches the free radical R· with the resulting radical A· assumed to be inactive toward monomer (i.e., unable to create a monomer radical). Assuming that the inhibitor A reacts fast and that the decomposition of the initiator is the limiting step, the rate of consumption of A will equal to the rate of appearance of R·, and the induction time is then given by the time required for all of the inhibitor A to be consumed.[47]

$$t_{\text{ind}} = {}^{[A]_o}\!/_{2fk_d[I]_o} \tag{2}$$

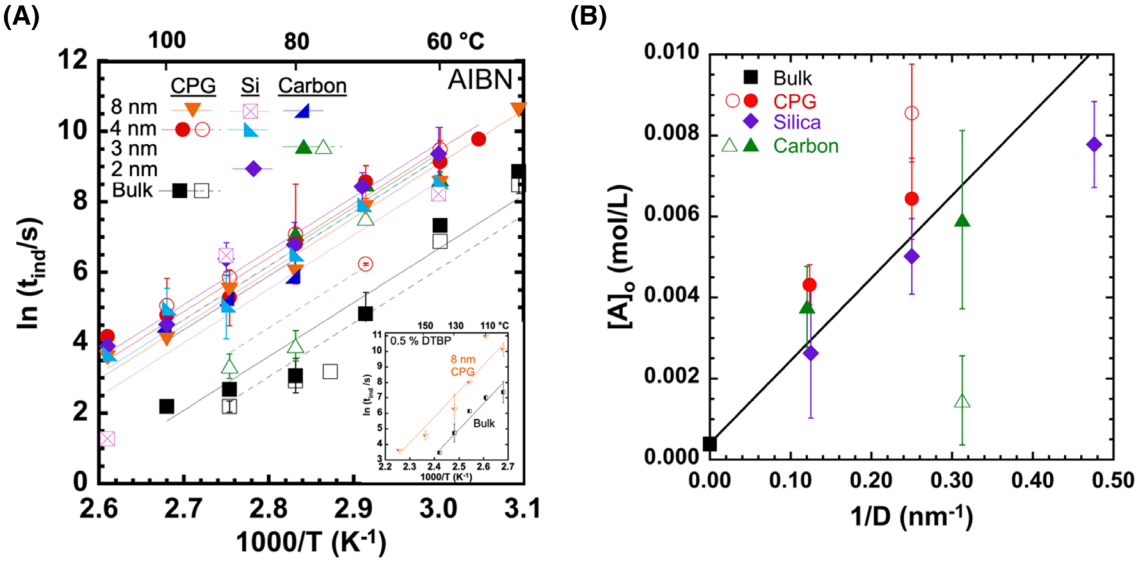

FIGURE 2 (A) The natural logarithm of the induction time for bulk and nanoconfined systems as a function of reciprocal temperature for 2,2′-azobisisobutyronitrile (AIBN)-initiated samples, where filled and open symbols represent samples initiated by 1.5 wt % and 2.5 wt % AIBN, respectively, with solid and dashed lines being Arrhenius fits using $E_a = 125$ kJ/mol to filled and open symbols; the inset is for di-tert-butyl peroxide systems with fits using $E_a = 139$ kJ/mol. (B) The calculated inhibitor concentration as a function reciprocal pore diameter for AIBN systems.

where $[A]_o$ and $[I]_o$ are the initial concentrations of inhibitor and initiator, f is the initiator efficiency, and k_d is the rate coefficient for dissociation of initiator. Taking the natural logarithm of both sides of Equation (2) and assuming an Arrhenius form for the rate coefficient with activation energy E_d and prefactor A_d indicates that the induction time should be linear with reciprocal temperature with a slope E_d/R:

$$\ln t_{ind} = {}^{E_d}\!/_{RT} + \ln\left({}^{[A]_o}\!/_{2f[I]_o A_d}\right) \quad (3)$$

Fitting the induction time data in Figure 2 to Equation (3) yields average E_d values of 125 ± 26 and 139 ± 20 kJ/mol for AIBN and DTBP, respectively, consistent with the reported literature values[47] of 123 and 147 kJ/mol for dissociation of AIBN and DTBP. Using the average E_d values to fit the data, we also obtain an estimate of the concentration of the presumed inhibitor $[A]_o$ in the sample. For the bulk reaction with AIBN, we find $[A]_o = (0.38 \pm 0.13) \times 10^{-3}$ mol/L assuming $f = 0.65$[48] and $A_d = 1.62 \times 10^{14}\ s^{-1}$,[47] which is consistent with the inhibitor being oxygen and consistent with the O_2 concentration in the bulk sample, which we measured to be 0.25×10^{-3} mol/L in the BzMA monomer at room temperature using a Elemental Instruments Firesting-GO2 oxygen meter (which has a reported accuracy of ±10%).[49] In the nanopore systems, the presumed inhibitor concentration $[A]_o$ increases linearly with reciprocal pore size, as shown in Figure 2B, which indicates the importance of the pore surface area. This also is consistent with the inhibitor being oxygen and consistent with the presence of physisorbed oxygen in the nanopores, which has been reported to be as high as 0.3 mol/L for nanoporous coal[50] and as high as 0.2 to 4 mol/L for mesoporous silica.[51] The fact that the inhibitor concentration is independent of the type of matrix also suggests that functional surface groups are not a primary source of inhibition; we have found that added trimethylsilanol does increase the induction time but only by a factor of 2.4 relative to the bulk for 24 wt % trimethylsilanol (which is equivalent to the silanol concentration in an 8 nm silica pore assuming that the CPG surface is akin to a fully hydroxylated silica surface, that is, having 4.9 OH groups/nm^2)[52] which is considerably less the factor of 10 that is found in all of the 8 nm nanopores.

Homogeneous radical chain polymerization is generally described by first order kinetics,[47] and at the early stages of the reaction, one can obtain an effective rate coefficient k_{eff} from the conversion versus time data:

$$-\ln(1-x) = k_{eff} t \quad (4)$$

where t is time after induction. In cases, where the equilibrium conversion does not approach unity because of thermodynamic limitations (e.g., as the ceiling temperature is approached and the rate of depropagation becomes significant relative to propagation), this equation should be rewritten as

$$-\ln(x_\infty - x) = k_{eff} t \quad (5)$$

where x_∞ is the equilibrium conversion. The initial effective rate coefficient can be related to the rate coefficient for the elementary steps involved in radical polymerization,[47] $k_{eff} = k_p\left(\frac{fk_d}{k_t}[I]_o\right)^{1/2}$, where k_p, k_d, and k_t are the rate coefficients for propagation, decomposition of the initiator, and termination, respectively, f refers to initiator efficiency, and $[I]_o$ is the initial concentration of initiator. Here, we obtain k_{eff} from the conversion versus temperature data in the low conversion regime, that is, <20% and prior to autoacceleration.

The natural logarithm of k_{eff} is plotted as a function of reciprocal temperature for systems containing 1.5 wt % AIBN in Figure 3A and for 2.5 wt % AIBN in Figure 3B. The effective rate coefficient increases as the reaction temperature increases, as expected, in the temperature range from 50 °C to 120 °C, and it is observed to be higher in the CPG and mesoporous silica nanopores than in bulk, with k_{eff} generally increasing as the pore size decreases and being higher in the mesoporous silica than in the CPG. Conversely, the rate in the carbon mesopores is less than that in the bulk and decreases as the pore size decreases. The dependence of k_{eff} on initiator concentrations and temperature is given by:

$$k_{eff} = [I]_o^{1/2} k_{ref} \exp\left[\left(\frac{1}{T_{ref}} - \frac{1}{T}\right)\frac{E_a}{R}\right] \quad (6)$$

where k_{ref} is the reference rate coefficient at the reference temperature, $T_{ref} = 373.15$ K, and E_a is the apparent activation energy. All of the data in Figure 3A,B are well described by Equation (6) and are fit using one value of k_{ref} and one value of E_a for a given reaction environment, as summarized in Figure 4A,B. The effective rate coefficients scale linearly with reciprocal pore size, with mesoporous silica showing the highest acceleration of the reaction under nanoconfinement, CPG showing intermediate acceleration, and ordered mesoporous carbon showing a decreased reaction rate. The activation energy of the bulk reaction is 76 ± 1 kJ/mol, whereas the E_a of nanoconfined reactions in CPG and ordered mesoporous carbon are lower than the bulk, consistent with our previous reports for *n*-alkyl methacrylates in CPG,[20,22,23] and roughly scaling with recriprocal pore size. On the other hand, the nanoconfined reactions in mesoporous silica have activation energies higher than the bulk except for the 8 nm pores, which is within error but smaller than the bulk value.

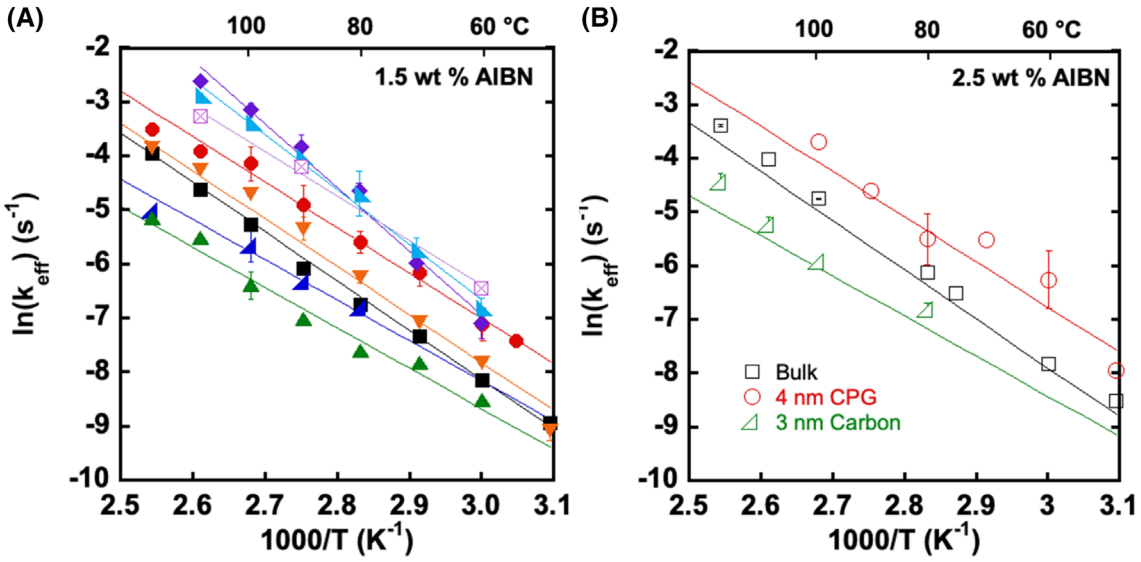

FIGURE 3 Natural logarithm of the effective rate coefficient k_{eff} versus 1000/T for BzMA initiated by (A) 1.5 wt % and (B) 2.5 wt % 2,2′-azobisisobutyronitrile with lines being linear fits of $ln(k_{eff})$ using the values of k_{ref} at 373.15 K and E_a reported in Figure 4.

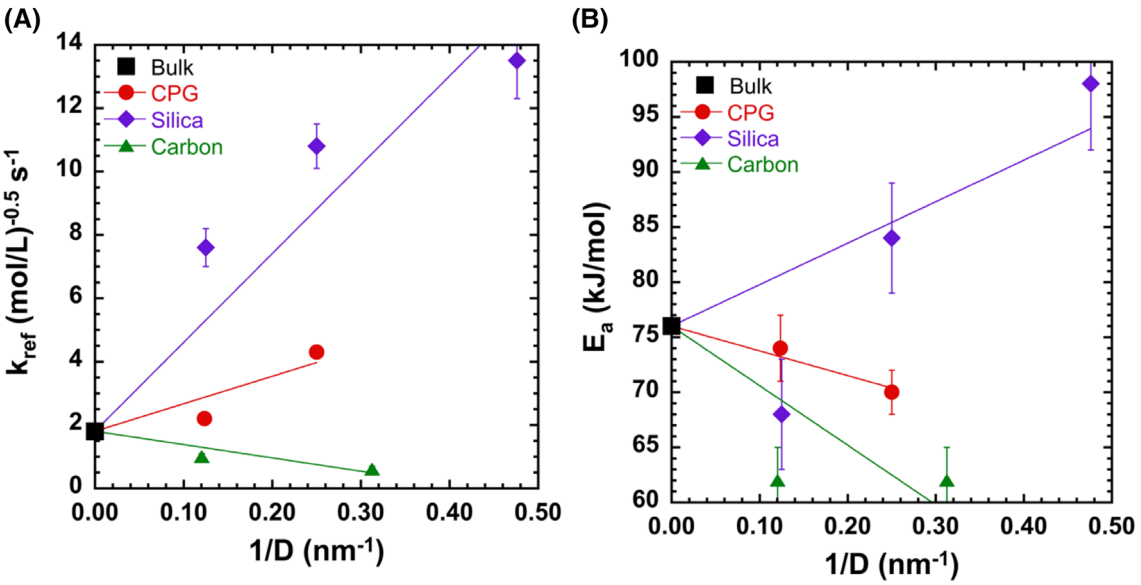

FIGURE 4 (A) Effective rate coefficient at 373.15 K and (B) activation energy versus reciprocal pore diameter. Lines are fits through the bulk value.

The effective rate coefficient at T_{ref} (373.15 K) in Figure 4A is nearly six times higher than the bulk when the reaction is performed in 4 nm mesoporous silica compared to bulk case and more than two times higher when performed in 4 nm CPG, whereas the rate coefficient in 3 nm carbon pores is a third of the bulk value. The rate coefficients are inversely proportional to the pore diameter D, suggesting that the rate is proportional to the pore surface to pore volume ratio and that changes are related to interactions between the monomer and the pore surface. We previously hypothesized[20,22,23] that the acceleration in native CPG might be due to the interaction between the methacrylate functionality of the reactant and silanol groups on the pore surface due to the fact that the polymerization is accelerated in native pores and not in pores in which the native silanol groups are replaced with trimethyl silyl[20]; hence as part of this work, we tested this hypothesis by adding trimethylsilanol to a mixture of BzMA monomer and AIBN initiator. Although we did find a small increase in induction time with added trimethylsilanol (TMS), the initial rate coefficient was constant within the error of the measurements (as shown in the Data S1), suggesting that the silanol groups on the native pore surface are not responsible for the catalytic effect observed.

Interestingly, the enhanced reactivity of BzMA in CPG is considerably weaker than that which we reported for MMA polymerization.[20] The weaker acceleration effect of CPG on the BzMA polymerization is presumably due to the higher hydrophobicity of BzMA compared to the MMA, EMA, and BMA with resulting weaker interactions between the BzMA and the native CPG pore surface relative, consistent with our recent findings on DMA.[23]

In the case of BzMA polymerization in mesoporous carbon, the effective rate coefficient decreases relative to the bulk value and is inversely proportional to pore diameter, as shown in Figure 4A, again indicating that the reduction of the polymerization rate may be attributable to functional groups on the carbon pore surface. There is no prior literature for polymerization in carbon mesopores, but the radical polymerization of butyl methacrylate (BMA) has been performed with graphene oxide (GO) as a nanoadditive. Achilias and co-workers[53,54] found that with the addition of GO, the polymerization rate of BMA decreases. Given the fact that the rate was inversely proportional to the amount of GO, the authors proposed that the hydroxyl groups on the surface of GO scavenge the primary radicals formed by the decomposition of the initiator, thus reducing initiator efficiency. Their hypothesis was also consistent with the higher molecular weight obtained in the presence of GO. In our study here, similar to the work of Achilias, we observe an increase in molecular weight in 8 nm carbon but only a very slight change in 3 nm carbon (as shown later). On the other hand, the presence of hydroxyl groups on solvents is found to increase the reaction rate,[55,56] and the hydroxyl group attached to silicon (silanol, which has a different acidity relative to a carbinol), does not seem to influence the reaction rate (as shown in the Data S1 for added TMS). Moreover, it is not clear why the activation energy should be reduced, as shown in Figure 4B, if the primary explanation for the rate decrease is a decrease in initiator efficiency. Hence, we suggest that more fundamental work is needed to clarify the mechanism responsible for the decrease in rate in our ordered mesoporous carbon.

Autoacceleration, also known as the Trommsdorff effect, occurs in radical polymerization due to the increase in viscosity as the reaction progresses, which suppresses the rate of termination relative to the rate of propagation. Autoacceleration is observed in the bulk polymerization in Figure 1 as an obvious increase in heat flow and a second exothermic peak starting at around 300 s. A much weaker degree of autoacceleration is seen for the nanoconfined samples in Figure 1, with no observable autoacceleration in the mesoporous silica samples presumably due their much higher initial reaction rates. The natural logarithm of the time to reach autoacceleration, t_{gel}, once the reaction begins (i.e., after subtracting the induction time) is shown in Figure 5A as a function of reciprocal temperature for the bulk and for reactions in CPG and mesoporous carbon initiated by AIBN, with the time (and conversion) required to reach autoacceleration defined as the point where the slope abruptly changes in a conversion versus time curve. Autoacceleration occurs at shorter times (after the induction period) in the CPG compared to the bulk, whereas polymerization in carbon mesopores requires longer times (after the induction period) to reach autoacceleration

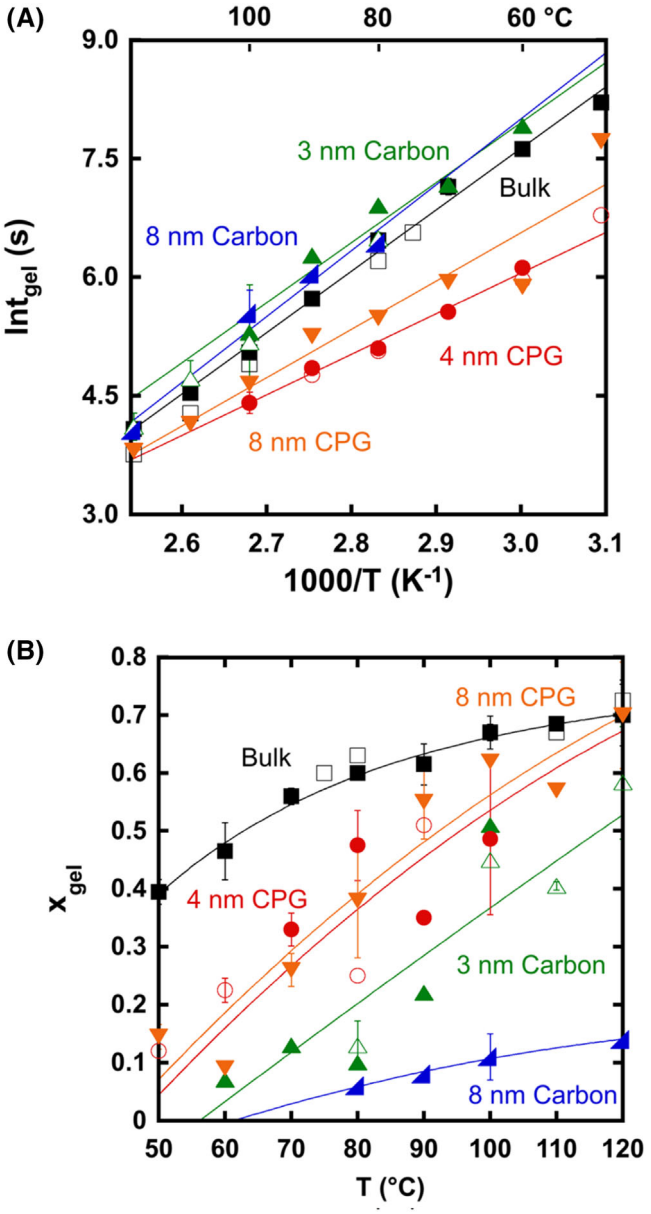

FIGURE 5 (A) Natural logarithm of the time to reach autoacceleration t_{gel} after the reaction begins (i.e., with the induction time subtracted) as a function of reciprocal temperature and (B) conversion to reach autoacceleration x_{gel} versus reaction temperature. Filled and open symbols represent the samples initiated by 1.5 wt % and 2.5 wt % 2,2′-azobisisobutyronitrile, respectively. Lines are only guides to the eye.

relative to the bulk. The difference in times to autoacceleration corresponds to the increase (or decrease, in the case of carbon) of the effective reaction rates relative to the bulk. Thus, the 8 nm CPG data lies between 4 nm and the bulk, and the 8 nm carbon lies between the 3 nm carbon and the bulk. All of the data follow Arrhenius behavior, and the apparent activation energies for the time to reach autoacceleration, t_{gel}, are found to be about 20 kJ/mol lower than the apparent activation energy for polymerization. There is no significant difference between the time to reach autoacceleration obtained from the two initiator concentrations (1.5 and 2.5 wt %).

The conversion required to reach autoacceleration is summarized in Figure 5B as a function of polymerization temperature. For all samples, x_{gel} increases as the temperature increases since the viscosity of the monomer/polymer solution decreases at higher temperatures at fixed composition, and hence, a higher conversion is needed to reach a viscosity that impacts the chain diffusivity and the rate of termination. The conversion needed to reach autoacceleration is highest for the bulk, and the required conversion decreases in the nanopores, presumably since the confined radicals have lower mobility leading to a suppression of the rate of termination relative to the rate of propagation. A similar result was previously reported for CPG-confined polymerization of *n*-alkyl methacrylates.[20,22] For AAO-confined polymerizations reported in the literature,[24–26] researchers have suggested that the rate of termination increases under nanoconfinement, but that does not seem to be the case in this work, since an increase in termination rate would be expected to increase the conversion required to reach autoacceleration, which we do not observe, and it would also lower the molecular weight, which we also do not observe. On the other hand, suppression of termination relative to propagation, which we suggest is dominant in our system, should lead to an increase in molecular weight of polymer synthesized under nanoconfinement, and this is our general observation, as will be shown later. We also note that experiments and simulations have shown an increase in viscosity (which would lead to lower diffusion) under nanoconfinement,[57–61] which is consistent with our interpretation of our results. Additionally, we note that although there are mechanisms that lower the effective viscosity of polymers in nanopores,[59–62] for example, due to plug flow under nanoconfinement,[59] slip at a pore surface,[61] or mobility at a free surface,[60] these latter mechanisms are not expected to dominate in our system since we do not have pressure-driven flow or a free surface.

The limiting or equilibrium conversion x_∞ (i.e., the conversion achieved at long reaction times) as a function of temperature is shown in Figure 6 for the three

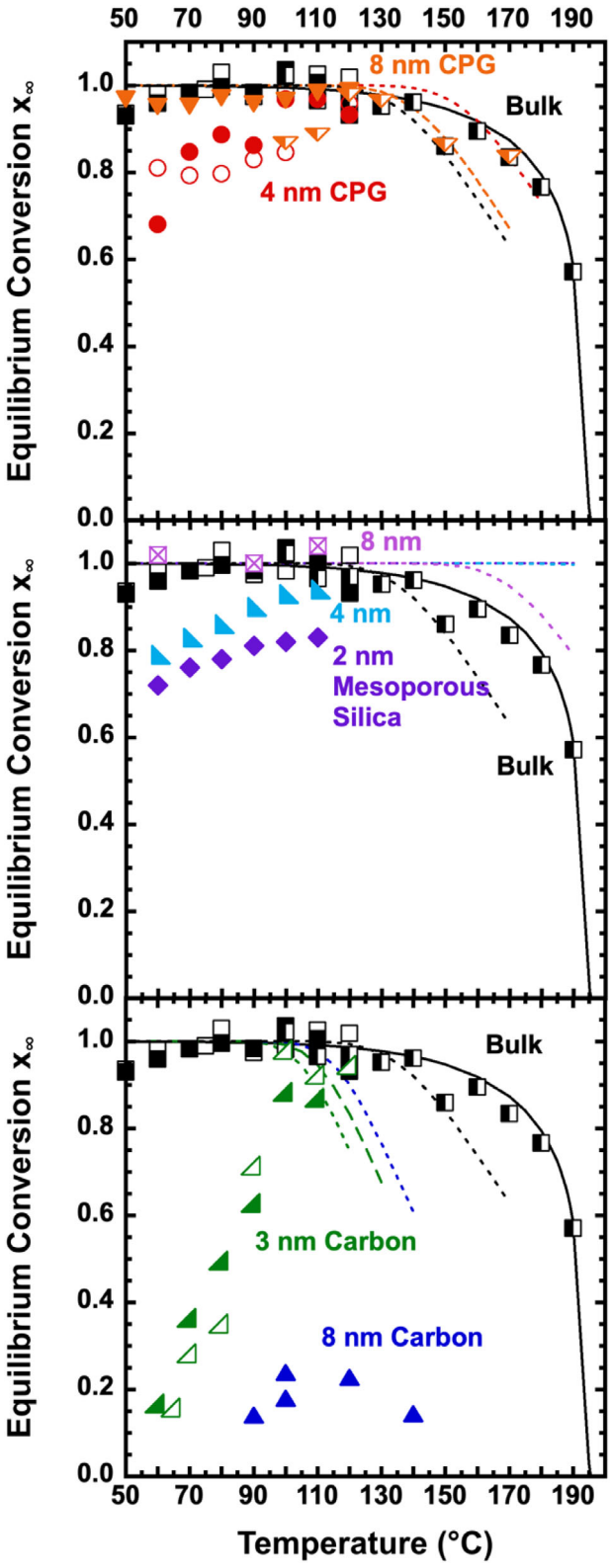

FIGURE 6 Equilibrium conversion (x_∞) versus temperature for bulk and nanoconfined samples in controlled pore glass, mesoporous silica, and ordered mesoporous carbon. Symbols are the same as used in Figure 2A. The short dashed lines indicate expectations for dead-end polymerization for 1.5% 2,2′-azobisisobutyronitrile (AIBN)-initiated systems and long dashed lines for 2.5% AIBN.

confinement matrices used. For bulk samples (shown by the black squares in each panel), nearly complete conversion is obtained at temperatures ≤120 °C; in this temperature range, AIBN is used as the initiator since its decomposition rate at these temperatures lies in an acceptable range.[47] On the other hand, in the high temperature range, where DTBP is used as initiator, the equilibrium conversion decreases as the temperature approaches the ceiling temperature ($T_c = 194$ °C) of poly(BzMA). For polymerization in 8 nm CPG and 8 nm mesoporous silica initiated by AIBN, nearly complete conversion is obtained at low temperatures, similar to the bulk. However, for 8 nm CPG initiated by DTBP, although the decrease of conversion in the high temperature range is observed to be similar to the bulk, on the low temperature side (<120 °C), the conversion is lower than the bulk, with the conversion decreasing as temperature decreases. A similarly decreasing conversion as temperature decreases is observed in AIBN-initiated reactions in 4 nm CPG, 2 and 4 nm mesoporous silica, and 3 nm ordered carbon mesopores. The data for 8 nm carbon seems to be different and this is attributed to the presence of small micropores (<2 nm) in this carbon due to the details of the synthesis. These small pores are estimated to comprise 64% of the total pore volume based on BET data as shown in the Data S1, and hence, we hypothesize that the volume of monomer in these smallest pores is dictating the limiting conversion observed. In fact, if we assume a limiting conversion of zero in the smallest pores, we estimate conversions of nearly unity (>95%) in the fraction of the large 8 nm carbon pores at the reaction temperatures from 80 °C to 120 °C, consistent with the 8 nm CPG and mesoporous silica data for AIBN-initiated samples.

A potential explanation for the observed limiting conversion at low temperature in Figure 6 is dead-end polymerization,[63] where monomer is left unreacted due to insufficient initiator concentration. The limiting conversion due to dead-end polymerization decreases with increasing temperature (contrary to our experimental observations) due to the fact that the activation energy for dissociation is higher than the effective activation energy for monomer consumption, with the relationship given by[47,63]

$$-\ln(1-x_\infty) = 2k_p\left(\frac{f}{k_d k_t}[I]_o\right)^{\frac{1}{2}} = \frac{2k_{\text{eff}}}{k_d} \qquad (7)$$

where k_{eff} is the quantity that we measure and show in Figure 3. Taking $k_d = A_d\ e^{-Ed/RT}$ and values from our work and the literature ($E_d = 123$ kJ/mol and $A_d = 1.62 \times 10^{14}$ s^{-1}),[47] predicted equilibrium conversions for the AIBN-initiated systems are shown in Figure 6 by the dashed lines. Dead-end polymerization is not expected to be relevant in CPG and mesoporous silica systems at temperatures below 120 °C, and it is not relevant in the carbon systems below 100 °C. We suggest that the limiting conversion at low temperatures may reflect thermodynamic limitations related to the monomer-polymer equilibria in nanoconfinement; further work is needed to fully understand this intriguing finding.

The degree of polymerization, N, is measured for the PBzMA synthesized in bulk and in the CPG and carbon mesoporous nanopores. Molecular weight increases as the temperature decreases in all cases examined, as shown in Figure 7. For products synthesized using 0.5 wt % DTBP as initiator, a higher molecular weight is obtained, with N being similar for bulk and 8 nm CPG. For AIBN-initiated samples, longer chains are formed under nanoconfinement compared to bulk polymerization except in 3 nm carbon for the 2.5 wt % AIBN where molecular weights are similar to the bulk. Theoretically, for a given reaction system, prior to autoacceleration, chains should be ~30% longer for monomer systems with 1.5 wt % AIBN compared to those with 2.5 wt % AIBN, which is observed here in the 3 nm carbon data, but no significant difference is observed in 4 nm CPG. We noted previously that our hypothesis that earlier autoacceleration (i.e., at lower

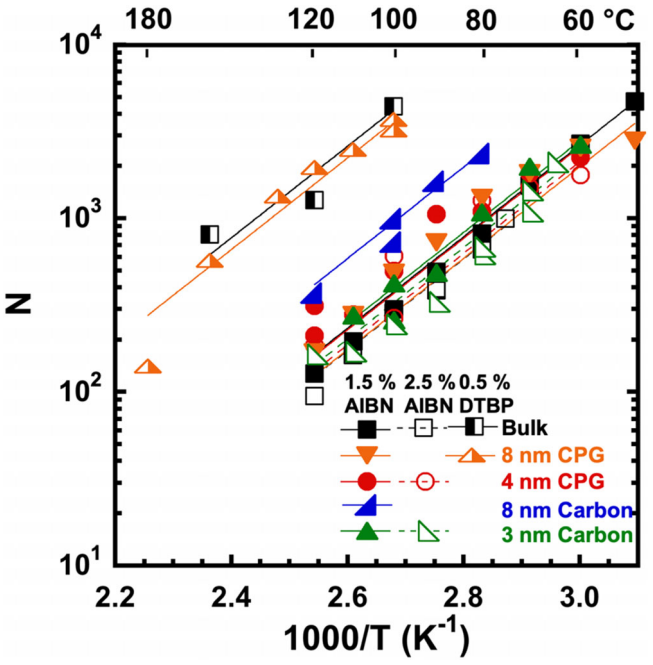

FIGURE 7 Degree of polymerization N versus reciprocal temperature for bulk and nanoconfined samples in controlled pore glass and ordered mesoporous carbon for initiator systems indicated in legend.

conversions) under nanonconfinement is attributable to suppression of termination relative to propagation would also lead to higher molecular weights for polymer synthesized under nanoconfinement. Indeed, this is observed at temperatures above 60 °C for five of the seven samples investigated with the other two samples (0.5% DTBP and in 8 nm CPG and 2.5% AIBN in 3 nm carbon) showing no appreciable difference from the bulk. At the lowest temperatures studied, 50 °C and 60 °C, the molecular weight of nanoconfined samples is equal to or lower than the bulk. This latter finding may be related to the limiting conversions observed in Figure 6, and future work will be aimed at understanding this result.

One of our aims for examining CPG, mesoporous silica, and ordered mesoporous carbon as nanoconfinement media was to elucidate the role of nanoconfinement versus nanopore surface functionality. Based on the results shown, it is clear that nanoconfinement has important effects, particularly on autoacceleration, equilibrium conversion, and molecular weight. The earlier conversion for autoacceleration and higher molecular weights are both attributed to decreased chain diffusivity in the pores and a concomitant decrease in the rate of termination. The surface to volume area, on the other hand, appears to be related to the induction time with little influence on matrix type, presumably due to physisorbed oxygen, whereas the effective rate of reaction seems to be related surface functionality, with the highest acceleration in mesoporous silica, intermediate acceleration in CPG, and a reduction of rate in ordered mesoporous carbon. This conclusion is also consistent with the differences observed in MMA polymerization in native CPG (in which the reaction was accelerated) versus in functionalized CPG where the surface was modified by replacing the native silanol groups with trimethyl silyl and where the reaction rate was the same as the bulk.[20] Interestingly in this work, although polymerization in mesoporous carbon is slower than the bulk, presumably due to a retardation effect of the pore surface, we still observe a lower conversion required to attain autoacceleration and higher molecular weights, which are attributable to confinement effects associated with decreased chain diffusivity under nanoconfinement.

4 | CONCLUSIONS

Radical polymerization of BzMA has been investigated in 2–8 nm-diameter native CPG, mesoporous silica, and ordered mesoporous carbon using differential scanning calorimetry (DSC). Induction times are longer for nanoconfined samples and are attributed to inhibition since induction has the same activation energy as for initiation but with opposite sign. The polymerization rate is found to be highest in mesoporous silica and also accelerated in CPG relative to bulk, increasing linearly with reciprocal pore diameter, but the acceleration of the BzMA polymerization in CPG is weaker than that found in our previous work on MMA, EMA, and BMA, presumably due to increased hydrophobicity of BzMA and a concomitant weaker interaction between the BzMA and the native pore surface. On the other hand, in carbon mesopores, the reaction rate relative to that in the bulk decreases linearly with reciprocal pore diameter, indicating a retardant effect of the pore surface. Similar to the bulk polymerization, the rate is proportional to initiator concentration to the one-half power. The apparent activation energies of the overall reaction rate in mesoporous silica is higher than the bulk, whereas those in CPG and carbon are lower than the bulk, with all seeming to scale roughly with reciprocal pore diameter. Autoacceleration is not observable in the mesoporous silica systems presumably due to the high initial reaction. On the other hand, in CPG and ordered mesoporous carbon, the time and conversion required to reach autoacceleration are lower in nanopores, and this effect is thought to be a nanoconfinement effect related to the limited diffusivity of radicals which then suppresses the rate of termination relative to propagation. Limiting conversions at low temperatures in the smallest nanopore systems (2 and 4 nm silica, 4 nm CPG, and 3 nm carbon for AIBN-initiated systems and 8 nm CPG for DTBP-initiation) decrease with decreasing temperature, and this effect, which is shown to not be due to dead-end polymerization, is intriguing and potentially reflects thermodynamic limitations related to the monomer-polymer equilibria in nanoconfinement. The PBzMA synthesized in CPG and 8 nm carbon with AIBN have higher molecular weights than those synthesized in bulk, consistent with suppression of termination relative to propagation at the nanoscale; however, at the lowest reaction temperatures, molecular weights are lower than the bulk, and this may be related to the decrease in limiting conversion.

ACKNOWLEDGMENTS

The authors gratefully acknowledge the funding from the National Science Foundation DMR-2141221, DMR-2004960, and DMR-1610614 (CHZ and SLS), CBET-1510612 and CBET-1336057 (BDV), and the Horn Professorship of Texas Tech University (SLS). We also acknowledge Prof. Kristin Hutchins for help with the GPC measurements. The authors thank Sarang M. Bhaway and Meeta Trivedi for their efforts on the

synthesis and characterization of the mesoporous carbon samples.

ORCID

Chunhao Zhai https://orcid.org/0000-0003-2410-8748
Yung P. Koh https://orcid.org/0000-0001-5140-1865
Bryan D. Vogt https://orcid.org/0000-0003-1916-7145
Sindee L. Simon https://orcid.org/0000-0001-7498-2826

REFERENCES

[1] C. L. Jackson, G. B. McKenna, *J. Chem. Phys.* **1990**, *93*, 9002.
[2] S. X. Cheng, G. B. McKenna, *Mol. Pharm.* **2019**, *16*, 856.
[3] K. M. Unruh, T. E. Huber, C. A. Huber, *Phys. Rev. B: Condens. Matter* **1993**, *48*, 9021.
[4] C. L. Jackson, G. B. McKenna, *J. Non-Crys. Solids.* **1991**, *131*, 221.
[5] Y. P. Koh, S. L. Simon, *J. Phys. Chem. B.* **2010**, *114*, 7727.
[6] S. Y. Gao, Y. P. Koh, S. L. Simon, *Macromolecules* **2013**, *46*, 562.
[7] E. Lopez, S. L. Simon, *Macromolecules* **2015**, *48*, 4692.
[8] J. L. Keddie, R. A. L. Jones, R. A. Cory, *Europhys. Lett.* **1994**, *27*, 59.
[9] P. B. Zetterlund, D. R. D'hooge, *Macromolecules* **2019**, *52*, 7963.
[10] M. J. Monteiro, M. F. Cunningham, *Macromolecules* **2012**, *45*, 4939.
[11] R. G. Gilbert, *Emulsion Polymerization: A Mechanistic Approach*, Academic Press, London **1995**.
[12] H. Y. Zhao, S. L. Simon, *Polymer* **2020**, *211*, 123112.
[13] S. Amanuel, V. M. Malhotra, *J. Appl. Polym. Sci.* **2006**, *99*, 3183.
[14] B. Sanz, N. Ballard, Á. Marcos-Fernández, J. M. Asua, C. Mijangos, *Polymer* **2018**, *140*, 131.
[15] Y. P. Koh, S. L. Simon, *J. Phys. Chem. B.* **2011**, *115*, 925.
[16] Q. X. Li, S. L. Simon, *Macromolecules* **2008**, *41*, 1310.
[17] Q. X. Li, S. L. Simon, *Macromolecules* **2009**, *42*, 3573.
[18] M. Tarnacka, M. Dulski, S. Starzonek, K. Adrjanowicz, E. U. Mapesa, K. Kaminski, M. Paluch, *Polymer* **2015**, *68*, 253.
[19] M. Malvaldi, S. Bruzzone, F. Picchioni, *J. Phys. Chem. B* **2006**, *110*, 12281.
[20] H. Y. Zhao, S. L. Simon, *Polymer* **2011**, *52*, 4093.
[21] H. Y. Zhao, S. L. Simon, *Polymer* **2015**, *66*, 173.
[22] Q. Tian, H. Y. Zhao, S. L. Simon, *Polymer* **2020**, *205*, 122868.
[23] Q. Tian, Y. P. Koh, S. V. Orski, S. L. Simon, *Macromolecules* **2022**, *55*, 8723.
[24] J. M. Giussi, I. Blaszczyk-Lezak, M. Susana Cortizo, C. Mijangos, *Polymer* **2013**, *54*, 6886.
[25] M. Salsamendi, N. Ballard, B. Sanz, J. M. Asua, C. Mijangos, *RSC Adv.* **2015**, *5*, 19220.
[26] M. Tarnacka, P. Maksym, A. Zieba, A. Mielanczyk, M. Geppert-Rybczynska, L. Leon-Boigues, C. Mijangos, K. Kaminski, M. Paluch, *Chem. Commun.* **2019**, *55*, 6441.
[27] H. C. Lee, J. Hwang, U. Schilde, M. Antonietti, K. Matyjaszewski, B. V. K. J. Schmidt, *Chem. Mater.* **2018**, *30*, 2983.
[28] M. Tarnacka, A. Dzienia, P. Maksym, A. Talik, A. Zięba, R. Bielas, K. Kaminski, M. Paluch, *Macromolecules* **2018**, *51*, 4588.
[29] A. G. Kalampounias, K. S. Andrikopoulos, S. N. Yannopoulos, *J. Chem. Phys.* **2003**, *119*, 7543.
[30] X. C. Li, T. A. King, F. Pallikari-Viras, *J. Non-Cryst. Solids* **1994**, *170*, 243.
[31] S. M. Ng, S. Ogino, T. Aida, K. A. Koyano, T. Tatsumi, *Macromol. Rapid Commun.* **1997**, *18*, 991.
[32] T. Uemura, Y. Ono, K. Kitagawa, S. Kitagawa, *Macromolecules* **2008**, *41*, 87.
[33] H. Y. Zhao, Z. N. Yu, F. Begum, R. C. Hedden, S. L. Simon, *Polymer* **2014**, *55*, 4959.
[34] F. Begum, H. Y. Zhao, S. L. Simon, *Polymer* **2012**, *53*, 3261.
[35] F. Begum, H. Y. Zhao, S. L. Simon, *Polymer* **2012**, *53*, 3238.
[36] D. Gu, F. Schüth, *Chem. Soc. Rev.* **2014**, *43*, 313.
[37] Y. F. Shi, Y. Wan, D. Y. Zhao, *Chem. Soc. Rev.* **2011**, *40*, 3854.
[38] M. R. Benzigar, S. N. Talapaneni, S. Joseph, K. Ramadass, G. Singh, J. Scaranto, U. Ravon, K. Al-Bahily, A. Vinu, *Chem. Soc. Rev.* **2018**, *47*, 2680.
[39] Z. Qiang, Y. F. Xia, X. H. Xia, B. D. Vogt, *Chem. Mater.* **2017**, *29*, 10178.
[40] W. Haller, *Nature* **1965**, *206*, 693.
[41] Y. Meng, D. Gu, F. Q. Zhang, Y. F. Shi, L. Cheng, D. Feng, Z. X. Wu, Z. X. Chen, Y. Wan, A. Stein, D. Y. Zhao, *Chem. Mater.* **2006**, *18*, 4447.
[42] M. Trivedi, F. Peng, X. H. Xia, P. I. Sepulveda-Medina, B. D. Vogt, *Langmuir* **2019**, *35*, 14049.
[43] Z. Qiang, Y. M. Chen, Y. F. Xia, W. F. Liang, Y. Zhu, B. D. Vogt, *Nano Energy* **2017**, *32*, 59.
[44] C. L. Jackson, G. B. McKenna, *Chem. Mater.* **1996**, *8*, 2128.
[45] L. J. K. Tong, W. O. Kenyon, *J. Am. Chem. Soc.* **1945**, *67*, 1278.
[46] D. W. van Krevelen, K. T. Nijenhuis, *Properties of Polymers: Their Correlation with Chemical Structure; Their Numerical Estimation and Prediction from Additive Group Contributions*, Elsevier, Oxford **2009**.
[47] G. Odian, *Principles of polymerization*, John Wiley & Sons, New York **2004**.
[48] G. Moad, *Prog. Polym. Sci.* **2019**, *8*, 130.
[49] P. Sulzer, R. Lebl, C. O. Kappe, T. Mayr, *React. Chem. Eng.* **2019**, *4*, 2081.
[50] B. Tan, G. Cheng, X. M. Zhu, X. B. Yang, *Sci. Rep.* **2020**, *10*, 6946.52.
[51] Y. L. He, X. Q. Hu, M. X. Xu, A. M. C. Ng, A. B. Djurisic, *Microporous Mesoporous Mater.* **2021**, *327*, 111426.
[52] L. T. Zhuravlev, *Colloids Surf., A* **2000**, *173*, 1.
[53] M. Michailidis, G. D. Verros, E. A. Deliyanni, E. G. Andriotis, D. S. Achilias, *J. Polym. Sci. Part A: Polym. Chem.* **2017**, *55*, 1433.
[54] I. S. Tsagkalias, S. Papadopoulou, G. D. Verros, D. S. Achilias, *Ind. Eng. Chem. Res.* **2018**, *57*, 2449.
[55] M. D. Zammit, T. P. Davis, G. D. Willett, K. F. O'Driscoll, *J. Polym. Sci. Part A: Polym. Chem.* **1997**, *35*, 2311.
[56] K. F. O'Driscoll, M. J. Monteiro, B. Klumperman, *J. Polym. Sci. Part A: Polym. Chem.* **1997**, *35*, 515.
[57] J. J. Hor, H. N. Wang, Z. Fakhraai, D. Lee, *Macromolecules* **2018**, *51*, 5069.

[58] C. H. Tu, M. Steinhart, H. J. Butt, G. Floudas, *Macromolecules* **2019**, *52*, 8167.
[59] Y. Yao, H. J. Butt, G. Floudas, J. Zhou, M. Doi, *Macromol. Rapid Commun.* **2018**, *39*, 1800087.
[60] A. Shavit, R. A. Riggleman, *Soft Matter* **2015**, *11*, 8285.
[61] D. Feng, X. F. Li, X. Z. Wang, J. Li, T. Zhang, Z. Sun, M. X. He, Q. Liu, J. Z. Qin, S. Han, *Chem. Eng. Sci.* **2018**, *186*, 228.
[62] L. G. Cencha, R. Urteaga, C. L. A. Berli, *Macromolecules* **2018**, *51*, 8721.
[63] A. V. Tobolsky, C. E. Rogers, R. D. Brickman, *Polymerization.* **1960**, *II*, 1277.

SUPPORTING INFORMATION

Additional supporting information can be found online in the Supporting Information section at the end of this article.

How to cite this article: C. Zhai, Y. P. Koh, B. D. Vogt, S. L. Simon, *J. Polym. Sci.* **2024**, 1. https://doi.org/10.1002/pol.20230332